

Cornering gapless quantum states via their torus entanglement

William Witczak-Krempa,¹ Lauren E. Hayward Sierens,^{2,3} and Roger G. Melko^{2,3}

¹*Department of Physics, Harvard University, Cambridge, MA 02138, USA*

²*Department of Physics and Astronomy, University of Waterloo, Ontario, N2L 3G1, Canada*

³*Perimeter Institute for Theoretical Physics, Waterloo, Ontario N2L 2Y5, Canada*

(Dated: August 16, 2021)

The entanglement entropy (EE) has emerged as an important window into the structure of complex quantum states of matter. We analyze the universal part of the EE for gapless systems put on tori in 2d/3d, denoted by χ . Focusing on scale invariant systems, we derive general non-perturbative properties for the shape dependence of χ , and reveal surprising relations to the EE associated with corners in the entangling surface. We obtain closed-form expressions for χ in 2d/3d within a model that arises in the study of conformal field theories (CFTs), and use them to obtain ansatzes without fitting parameters for the 2d/3d free boson CFTs. Our numerical lattice calculations show that the ansatzes are highly accurate. Finally, we discuss how the torus EE can act as a fingerprint of exotic states such as gapless quantum spin liquids, e.g. Kitaev’s honeycomb model.

Measures of quantum entanglement have emerged as powerful tools to characterize complex many-body systems,^{1–5} such as phases with topological order, gapless spin liquids and quantum critical states lacking long-lived excitations. The entanglement entropy (EE) and its Rényi relatives have proven especially useful. The EE of a spatial region A , heuristically, measures the amount of entanglement between the inside of A and the outside. Different regions will reveal different properties about the physical state. Generally, a convenient choice is to work on a space that is periodic in at least one direction, *i.e.* a cylinder or, particularly in the case of finite-size lattice calculations, a torus. In this setting, region A is often chosen to wrap around at least one cycle, making it topologically non-trivial. In a large class of topologically ordered systems in 2 spatial dimensions (2d), the EE of the groundstate on a cylinder or torus reveals a wealth of information^{6–8} about the fractionalized excitations (anyons). Furthermore, these EEs have proved to be useful diagnostics in the search for such exotic phases.^{9–12} In contrast, for gapless states, analytical^{3,13–22} and numerical^{14,23–28} studies have revealed that the situation is more intricate and numerous open questions remain.

In this work, we analyze the universal torus EE of gapless theories in 2d/3d. We focus our attention on scale invariant systems such as conformal field theories (CFTs) and Lifshitz quantum critical theories ($z \neq 1$), thus excluding the extra complexity due to Fermi surfaces. We derive general properties of the torus EE in 2d/3d using strong subadditivity²⁹ and other considerations. We then make new connections between the shape dependence of the torus EE, and the EE associated with sharp corners,² as shown in Fig. 1d. The comparison is natural because both quantities are expressed in terms of an angle variable. Surprisingly, we find that the angle dependence of both the torus and corner functions are nearly equal when properly normalized, Fig. 2. This is illustrated using free CFTs, and strongly coupled ones. To gain more intuition about the shape dependence of universal term, we derive a closed-form expression for the torus EE in

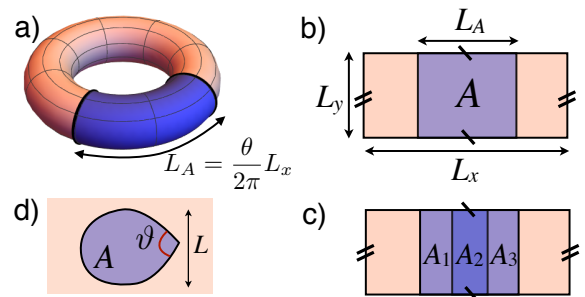


FIG. 1. **a & b)** 2d space with a torus topology. We study the EE of a cylindrical region A . **c)** Constraints on the torus EE function $\chi(\theta)$ result from dividing A into 3 parts, and applying strong subadditivity. **d)** Region with a sharp corner.

2d/3d using a CFT construction. This allows us to make approximate predictions for the free boson CFT, *without any fitting parameters*. Our numerical analysis shows that these predictions work accurately. We then discuss how the torus EE can be used to reveal both the topological and geometrical degrees of freedom of gapless spin liquids, using the Kitaev model as an example.

Fundamentals of torus entanglement: We consider a system on a flat torus, Fig. 1, *i.e.* we identify the coordinate r_i with $r_i + L_i$, $i = x, y$. Given the corresponding groundstate, we study its EE associated with a cylindrical region A of length L_A , $S(A) = -\text{tr}(\rho_A \ln \rho_A)$; ρ_A is the reduced density matrix of A . The EE scales as

$$S(A) = \mathcal{B} 2L_y/\delta - \chi + O(\delta/L_y), \quad (1)$$

in the limit where L_i, L_A far exceed the microscopic (UV) scale δ , which can be taken to be the lattice spacing. The first term corresponds to the “area law”, with a non-universal prefactor \mathcal{B} . Our interest lies in the δ -independent term, $-\chi$, because it is *universal*. It remains constant with growing L_y , at fixed ratios L_A/L_i , but in general depends non-trivially on both ratios. χ thus constitutes a non-trivial measure of the low-energy degrees

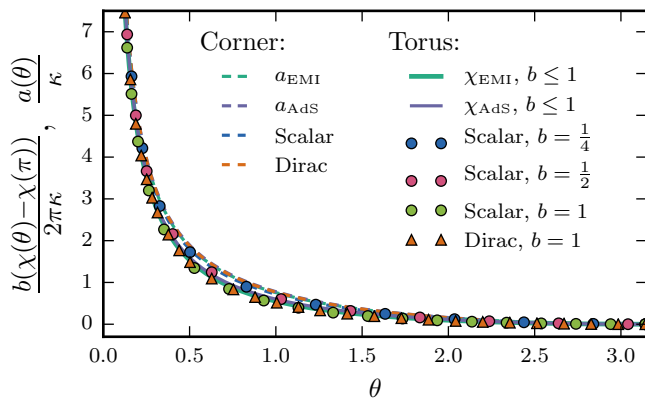


FIG. 2. Comparing the universal torus and corner EE of various CFTs in 2d.

of freedom of the system, and as we shall see, acts as fingerprint of the state.

We now obtain non-perturbative properties of the torus function $\chi(\theta; b)$, where we have defined the natural angular variable $\theta = 2\pi L_A/L_x$, and the aspect ratio $b = L_x/L_y$ (we shall often keep the b -dependence implicit). First, since we are dealing with pure states, the EE of A must equal that of its complement, *i.e.* $\chi(\theta) = \chi(2\pi - \theta)$; we shall henceforth restrict ourselves to $0 < \theta \leq \pi$, as in Fig. 2. Further, since the limit where A approaches half the torus is not singular, χ will be analytic about π :

$$\chi(\theta \approx \pi) = \sum_{\ell=0} c_{\ell} \cdot (\pi - \theta)^{2\ell}, \quad (2)$$

where only even powers appear due to the aforementioned reflection symmetry about π . The c_{ℓ} depend on the aspect ratio b , and it would be interesting to understand which properties of the state they encode. To derive further constraints on χ , we invoke an important property of the EE, namely its strong subadditivity²⁹ (SSA), which implies the following inequality for 3 non-overlapping regions: $S(A_1 \cup A_2 \cup A_3) + S(A_2) \leq S(A_1 \cup A_2) + S(A_2 \cup A_3)$. The key idea is to divide A into 3 regions as in Fig. 1c, with angles θ_i , and apply SSA. Substituting Eq. (1) into the SSA inequality, we find that the boundary law contributions cancel and we are left with $\chi(\theta_1 + \theta_2 + \theta_3) + \chi(\theta_2) \geq \chi(\theta_1 + \theta_2) + \chi(\theta_2 + \theta_3)$. From this, we can derive

$$\chi'(\theta) \leq 0, \quad \chi''(\theta) \geq 0, \quad (3)$$

for $0 < \theta \leq \pi$, *i.e.* the torus function $\chi(\theta)$ is convex decreasing on that interval. As a direct consequence of the inequalities (3), the second expansion coefficient in Eq. (2) satisfies $c_1 \geq 0$ (for all aspect ratios).

We now examine the limit $\theta \rightarrow 0$ with $L_{x,y}$ fixed, in which case the EE reduces to that of a (periodic) thin strip of width $L_A \rightarrow 0$ and length $L_y \gg L_A$. We argue that the periodicity in the x, y -directions and the associated

boundary conditions do not influence χ in this limit since the EE is dominated by degrees of freedom that do not exceed length scales $\sim L_A \ll L_{x,y}$. The total χ can be obtained by adding the contributions from these local patches, and will be proportional to L_y/L_A . We can thus relate the thin slice limit on the torus to the EE of a thin strip in *infinite* space. For scale invariant systems, this reads² $S_{\text{strip}} = \mathcal{B}2L/\delta - \kappa L/L_A$, where L_A is the strip's width. L is the long-distance regulator of the infinite strip; alternatively, we can define the EE per unit length, S_{strip}/L . χ will thus have the same $\kappa L_y/L_A$ divergence in the thin slice limit:

$$\chi(\theta \rightarrow 0) = \kappa \frac{L_y}{L_A} = \frac{2\pi\kappa}{b\theta}. \quad (4)$$

Further, by virtue of (3), $\kappa \geq 0$. This means that in the small- θ limit the full EE, Eq. (1), decreases since the universal contribution χ appears with a negative sign. This is consistent since when A vanishes, $S=0$. The universal constant κ has been computed for certain critical theories;³⁰ it will play a central role in our discussion.

Relation to corner entanglement: The above properties share striking similarities with the EE associated with sharp corners, as we now explain. Given a region A in the infinite plane that contains a corner with opening angle ϑ , Fig. 1d, the EE scales as

$$S(A) = B L/\delta - a(\vartheta) \ln(L/\delta) + \dots, \quad (5)$$

where B is the area law prefactor, and $a(\vartheta)$ is a *universal* coefficient arising from the corner.^{13,30-34} It encodes rich low-energy information about the state,^{5,13,26,33,35-39} but in contrast to χ , it vanishes for gapped systems and is thus blind to purely topological degrees of freedom. $a(\vartheta)$ is also symmetric about π (at which point the corner disappears), and can be expanded as in Eq. (2). For CFTs, the leading term in the expansion is^{35,40,41} $(\pi^2 C_T/24)(\pi - \vartheta)^2$, where C_T determines the 2-point function of the stress tensor (and thus of the energy density) in the groundstate. Fig. 2 shows $a(\vartheta)$ for the free scalar/Dirac fermion³⁰ and holographic CFTs.³² Further, $a(\vartheta)$ obeys the same monotonicity and convexity conditions³² (3). Finally, in the sharp corner limit $\vartheta \rightarrow 0$, the corner function shows a $1/\vartheta$ divergence³⁰ just as χ : $a(\vartheta \rightarrow 0) = \kappa_c/\vartheta$. For CFTs, $\kappa_c = \kappa$ is exactly the same universal constant that controls the divergence of $\chi(\theta \rightarrow 0)$, Eq. (4). This holds because the sharp corner geometry can be conformally mapped to that of a thin strip,⁴⁰ which controls $\chi(\theta \rightarrow 0)$ as discussed above. It would be interesting to see if non-conformal critical theories ($z \neq 1$) have the same relation between their sharp-corner κ_c and thin-slice coefficients κ .

Given the similar asymptotics of $\chi(\theta)$ and $a(\vartheta)$, one can wonder how they compare at intermediate angles. Fig. 2 shows the torus and corner functions of various CFTs. For a meaningful comparison, we normalize them by the thin-slice/sharp-corner coefficient κ . Surprisingly, all curves nearly overlap in the entire range of angles.

What makes the collapse more remarkable is that the curves for the holographic CFTs²¹ and the Extensive Mutual Information model^{42,43} (defined below) hold for *all* aspect ratios $b \leq 1$ (App. A 4), a non-trivial fact in itself. The same b -independence of $b\chi$ approximately holds for the massless scalar, as we illustrate with numerical data at $b=1, \frac{1}{2}, \frac{1}{4}$, taken from Fig. 3. The reason for the collapse constitutes an open question beyond the scope of this work, but it suggests a deeper relation between wavefunctions on spaces with different topologies/geometries.

Ansatz from extensive mutual information: To gain further intuition about the EE on tori, we derive a closed-form ansatz for $\chi(\theta)$ that can be meaningfully compared with a large class of gapless states, particularly CFTs. To do so we use the Extensive Mutual Information model (EMI),^{42–44} which has proven useful in the analysis of the EE of CFTs in various dimensions.^{35,36,42–44} The EMI is not defined through a Hamiltonian, but instead allows for a simple geometric computation of the EE within the bounds of conformal symmetry, and has passed numerous non-trivial tests.^{35,36,42,44} The resulting EE of the EMI can be interpreted⁴⁴ in terms of an ansatz for twist (or swap) operators used to compute Rényi and entanglement entropies. The designation EMI comes from the fact that its mutual information $I(A, B) = S(A) + S(B) - S(A \cup B)$ is extensive: $I(A, B \cup C) = I(A, B) + I(A, C)$. In infinite flat space, the EE of a region A can be computed as follows within the EMI:

$$S(A) = \int_{\partial A} d\mathbf{r}_1 \int_{\partial A} d\mathbf{r}_2 \hat{n}_1 \cdot \hat{n}_2 C(\mathbf{r}_1 - \mathbf{r}_2), \quad (6)$$

where $\hat{\mathbf{n}}$ denotes the unit normal to the boundary ∂A , and $C(\mathbf{r}) = s_1/|\mathbf{r}|^{2(d-1)}$. The coordinates $\mathbf{r}_{1,2}$ live on ∂A , and s_1 is a positive constant. In order to apply the prescription (6) to the torus, we need to account for the periodicity when determining the function C . However, contrary to the infinite plane, conformal invariance and the extensivity of the mutual information do not suffice to fix C on the torus, and one is left with a richer set of possibilities. A simple choice for C is described in App. A; the resulting torus EE reads:

$$\chi_{\text{EMI}}(\theta) = 4\kappa \left[\frac{\cot^{-1}\left(\frac{b}{\pi}\theta\right)}{b\theta} + \frac{\cot^{-1}\left(\frac{b}{\pi}(2\pi - \theta)\right)}{b(2\pi - \theta)} \right] + 2\gamma \quad (7)$$

where $\cot^{-1} z$ is the inverse cotangent, and γ is a constant. We have normalized the first term of (7) using κ so as to reproduce the expected small θ divergence, Eq. (4). χ_{EMI} is thus non-negative for all angles and aspect ratios. Our result is naturally symmetric and analytic about $\theta = \pi$, as in Eq. (2), and obeys the constraints (3) from SSA. Eq. (7) thus provides a closed-form candidate function to analyze the EE of strongly interacting states, especially CFTs, on tori. This is a powerful tool since virtually no other analytic results exist in this case. In an important development, a semi-analytical result was

obtained²¹ for χ in special CFTs using the holographic AdS/CFT correspondence. However, singular behavior was found as the aspect ratio goes through $b=1$. Such non-analyticities are not expected for generic CFTs, as in the quantum critical Ising model, and are indeed absent in Eq. (7) and in the free boson CFT (Fig. 3). Nevertheless, as noted above, striking similarities exist for $b \leq 1$ between the EMI and AdS functions, Fig. 2. In the latter case $b \cdot (\chi - \chi(\pi))$ is exactly independent of b ,²¹ while for the EMI, this holds to excellent accuracy and is not a priori obvious from Eq. (7), see App. A 4 for more details.

A useful limit to consider is the thin torus: $b \rightarrow \infty$ with θ fixed, in which case Eq. (7) reduces to $2\gamma + O(b^{-2})$. Namely, the universal EE approaches a pure constant independent of L_A, L_i , which is twice the universal EE associated with a semi-infinite cylindrical bipartition of an infinite cylinder (App. A). This is consistent with the expectation that a generic CFT will not contain gapless modes in the 1d limit because the contracting y -direction leads to a large $\sim 1/L_y$ gap. Otherwise, the EE would scale as $\sim \ln\left[\frac{L_x}{\pi\delta} \sin\left(\frac{\pi L_A}{L_x}\right)\right]$ when L_A is changed, corresponding to the behavior of a critical 1d system on a circle.¹ The absence of such critical scaling in the thin torus limit is verified²¹ in the strongly coupled holographic CFTs mentioned above. Exceptions do occur, *e.g.* for non-interacting CFTs with *periodic* boundary conditions due to zero energy modes, but one can twist the boundary conditions to gap them out (see below).

3d torus: We now explore the largely uncharted territory of torus entanglement in gapless 3d theories. We take the subregion A to be a hyper-cylinder of length L_A aligned along x , Fig. 4. The corresponding angle variable is again $\theta = 2\pi L_A/L_x$. The analog of Eq. (1) in 3d reads:

$$S^{3d}(A) = \mathcal{B} \frac{2L_y L_z}{\delta^2} - \chi^{3d} + O(\delta/L_{y,z}), \quad (8)$$

where $\chi^{3d}(\theta; b_y, b_z)$ now depends on the 2 aspect ratios, $b_{y,z} = L_x/L_{y,z}$. The general properties obtained above for the 2d torus function χ can be adapted *mutatis mutandis* to the 3d case. In particular, χ^{3d} will be convex decreasing for $0 < \theta \leq \pi$, as in Eq. (3), and will be analytic about $\theta = \pi$. Further, in the small- θ limit we find

$$\chi^{3d}(\theta \rightarrow 0) = \kappa^{3d} \frac{L_y L_z}{L_A^2} = \frac{(2\pi)^2 \kappa^{3d}}{b_y b_z \theta^2} \quad (9)$$

since the EE effectively becomes that of an infinite thin slab with thickness L_A . Our 2d argument given above can be generalized to argue that the system is insensitive to the periodicity of the x, y, z directions in this limit. $\kappa^{3d} \geq 0$ is a universal constant characterizing the theory,³⁰ and it is the 3d analog of the 2d κ encountered above. As we have done in 2d, we can use the EMI to obtain a closed-form torus function $\chi_{\text{EMI}}^{3d}(\theta)$. Fig. 4 shows the result for different aspect ratios; the full answer is given in App. A.

Torus EE for lattice bosons: We numerically eval-

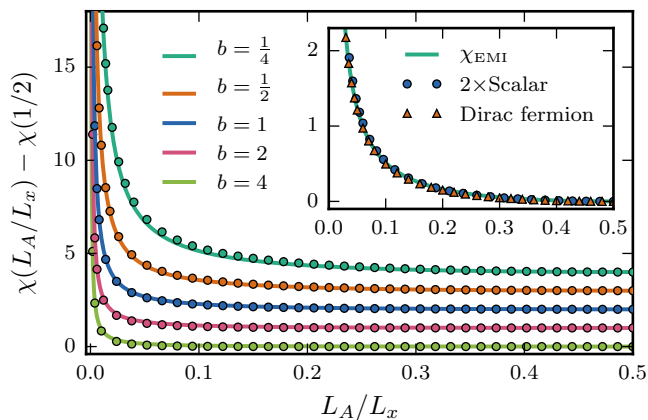


FIG. 3. **Main:** Torus function χ for the massless scalar in 2d for various aspect ratios $b = L_x/L_y$; it has been vertically offset for clarity. The points are numerical data, and the lines are the predictions obtained using χ_{EMI} , *without any fitting parameters*. **Inset:** Dirac fermion data²¹ at $b=1$, the corresponding χ_{EMI} , and the complex scalar data for comparison. The axes represent the same quantities as in the main plot.

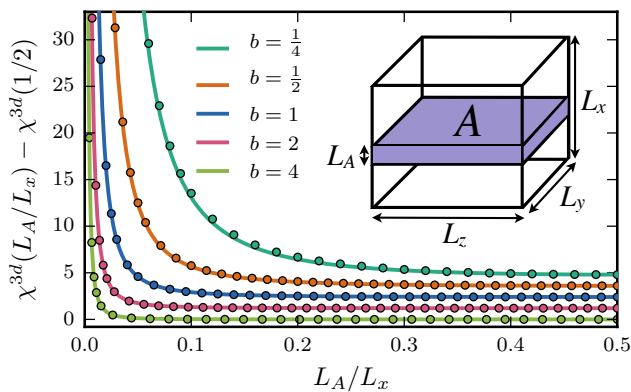


FIG. 4. **Main:** Torus function χ^{3d} for the massless free boson in 3d for various aspect ratios $b_y = b_z = b$. The points are the numerical data and the line is the prediction obtained using the ansatz χ_{EMI}^{3d} , *without any fitting parameters*. **Inset:** Opposing faces of the box are identified to give a 3-torus topology. Region A is a hyper-cylinder extending along x .

uate the torus EE of a free and massless relativistic boson (a CFT) in 2d/3d using the square/cubic lattice realization of the Hamiltonian $H = \int d^d x [\frac{1}{2} \pi^2 + \frac{1}{2} (\nabla \phi)^2]$, where ϕ is the 1-component boson and π its conjugate momentum. This theory corresponds to the Gaussian fixed point of the interacting quantum critical Ising model in 2d/3d, and constitutes a key benchmark system. We obtain the torus EE by directly evaluating the reduced density matrix of A from the two-point vacuum correlation functions $\langle \phi_{\mathbf{x}} \phi_{\mathbf{x}'} \rangle$ and $\langle \pi_{\mathbf{x}} \pi_{\mathbf{x}'} \rangle$ for lattice sites $\mathbf{x}, \mathbf{x}' \in A$;⁴⁵ details are given in App. B. We perform our 2d calculations on lattices of size $L_x = 500$, and our 3d calculations on lattices of size $L_x = 100, 140, 200, 288, 456$ for aspect ratios $b_y = b_z = \frac{1}{4}, \frac{1}{2}, 1, 2, 4$ (respectively). Each lattice

has antiperiodic boundary conditions (APBC) in the y -direction and PBC along the remaining directions. We use the former to avoid the $\mathbf{k} = 0$ zero mode present for PBC.

The numerical results in 2d/3d are shown in Figs. 3, 4, respectively. The solid lines in both figures correspond to the EMI candidate functions, Eq. (7) in 2d, while the 3d one is given in the appendix. Crucially, *no fitting* to the data has been performed. Instead, to generate the lines we have relied on two facts: First, the EMI torus functions relative to their value at $\theta = \pi$, $\chi_{\text{EMI}}^{3d}(\theta) - \chi_{\text{EMI}}^{3d}(\pi)$, depend on a single universal constant, κ^{3d} . Second, this constant has been computed in a *different* context for the massless scalar in 2d/3d:³⁰ $\kappa_{\text{sc}} = 0.0397$, $\kappa_{\text{sc}}^{3d} = 5.54 \times 10^{-3}$. The resulting ansatz curves and the data agree with each other exceptionally well, which is surprising since we have not done any fitting. The agreement in 2d/3d extends over a wide range of aspect ratios, meaning the ansatz even captures the b -dependence without any fitting! We note that since the EMI does not describe a free boson CFT, we expect that some of the deviations are intrinsic.

The inset of Fig. 3 shows the data for a massless free Dirac fermion (another CFT) obtained numerically in Ref. 21 with (A)PBC along $(y)x$. In this case, we again know the value of the small- θ constant,³⁰ $\kappa_{\text{Dirac}} = 0.0722$, which allows us to fix the χ_{EMI} ansatz; the result is the line in the inset of Fig. 3. We have also shown the data for a complex scalar, which overlaps almost exactly with that of the Dirac fermion. Part of the agreement can be explained from the fact that the complex scalar has $\kappa = 2\kappa_{\text{sc}} = 0.0794$, which is close to the Dirac value.

Summary & outlook: We have seen that the universal EE of cylindrical regions on tori reveals non-trivial information about scale invariant quantum systems, like conformal field theories, in 2d/3d. Our findings range from general non-perturbative properties to concrete examples involving bosons on a lattice. We note that many of these results can be extended to the Rényi entropies S_n . In particular, in the thin slice limit χ_n will show the same divergence as in Eqs. (4,9), but with κ_n . A torus function was previously derived⁴⁶ at $n \geq 2$ for a family of 2d Lifshitz quantum critical points,⁴⁷ and it was successfully compared with the von Neumann case in various theories. Many of our results apply to that function.⁴⁸

Since the torus EE can also capture topological information about the excitations⁶⁻⁸ (relating to anyons, say), it will be interesting to use it to obtain fingerprints for gapless spin liquids or deconfined quantum critical points. In this vein, a simple example where χ encodes both topological and geometrical degrees of freedom is Kitaev's gapless spin liquid on the honeycomb lattice.⁴⁹ In this frustrated spin model, the emergent long-distance degrees of freedom are 2 massless Majorana fermions coupled to a Z_2 gauge field. We expect the universal EE to be $\chi_f(\theta) + \chi_{\text{top}}$, owing to the factorization of the fermions and Z_2 contributions.⁵⁰ χ_{top} is purely topological and comes from the Z_2 gauge theory,⁷ while the fermions

yield the shape dependent $\chi_f(\theta)$. Inspired by this capability of χ to capture both topological and gapless degrees of freedom, we ask whether the torus EE can yield a RG monotone, in the same spirit as the disk EE^{51,52}?

Acknowledgments—We are thankful to P. Bueno, X. Chen, E. Fradkin, A. Lucas for useful discussions. WWK is grateful for the hospitality of Perimeter Institute, where this work was initiated. WWK was funded by a fellowship from NSERC, and by MURI grant W911NF-14-1-0003 from ARO. LHS was partially funded by the Ontario Graduate Scholarship. RM is supported by NSERC of Canada, the Canada Research Chair Program and the Perimeter Institute for Theoretical Physics. Research at Perimeter Institute is supported by the Government of Canada through the Department of Innovation, Science and Economic Development and by the Province of Ontario through the Ministry of Research & Innovation.

Supplementary Information

CONTENTS

A. Torus entanglement of the Extensive Mutual Information model	5
1. Infinite cylinder	6
2. Torus in 2d	6
3. Torus in 3d	7
4. Properties in $2d$	8
a. Special scaling for $b \leq 1$	8
b. Smooth and thin-torus limit expansions	8
5. Another ansatz	8
B. Numerical calculations	9
References	10

Appendix A: Torus entanglement of the Extensive Mutual Information model

Let us first recall the calculation of the EE within the Extensive Mutual Information model (EMI) for a region A in infinite flat space.^{42–44} One needs to evaluate the following double integral over two copies of the entangling surface ∂A :

$$S(A) = \int_{\partial A} d\mathbf{r}_1 \int_{\partial A} d\mathbf{r}_2 \hat{\mathbf{n}}_1 \cdot \hat{\mathbf{n}}_2 C(\mathbf{r}_1 - \mathbf{r}_2), \quad (\text{A1})$$

with

$$C(\mathbf{r}) = \frac{s_1}{|\mathbf{r}|^{2(d-1)}}, \quad (\text{A2})$$

where d is the spatial dimension, $\hat{\mathbf{n}}$ the vector normal to ∂A , and $\mathbf{r}_{12} = \mathbf{r}_1 - \mathbf{r}_2$ is the separation vector. The prescription given in Eq. (A2) cannot be applied to the

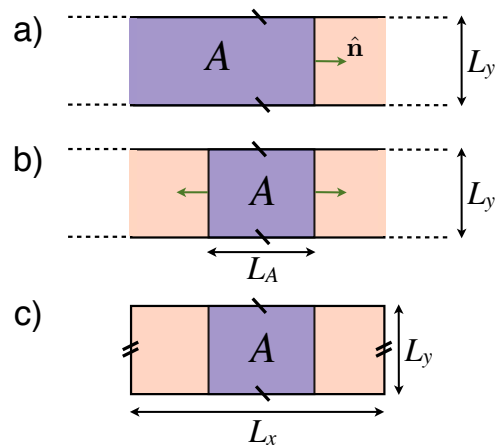


FIG. 5. a) Semi-infinite subregion A of a space with the topology of an infinite cylinder. b) Finite subregion A of the infinite cylinder. c) Finite subregion A of a space with a torus topology. Each green arrow denotes a normal vector, $\hat{\mathbf{n}}$, to the entangling surface.

torus because it does not account for the periodicity of space. On the torus we require $C(\mathbf{r})$ to be periodic along all the spatial directions. Further, at distances much shorter than the linear dimensions of the torus, L_i , the C -function needs to reduce to Eq. (A2), i.e.

$$C(r_i \ll L_i) = s_1/|\mathbf{r}|^{2(d-1)}, \quad (\text{A3})$$

because in this limit the boundary conditions of space should not affect the EE. This scaling naturally follows from the scale invariance of the system on the infinite plane.^{42–44} We note that under such general conditions, $S(A)$ defined in Eq. (A1) will have an extensive mutual information I for non-intersecting regions A, B, C living on the torus:

$$I(A, B \cup C) = I(A, B) + I(A, C) \quad (\text{A4})$$

where $I(A, B) = S(A) + S(B) - S(A \cup B)$. We are thus led to the conclusion that on the torus, the form of $C(\mathbf{r})$ is not entirely constrained by symmetry and extensivity of the mutual information. This is not very surprising because conformal symmetry on the torus is much less powerful than in infinite space \mathbb{R}^d . For instance, conformal symmetry in 1+1 Euclidean spacetime dimensions is not sufficiently powerful to fix the 2-point functions of local operators in a CFT on the torus; they will thus depend on many details of each given theory. In contrast, such correlation functions are fixed by symmetry on the infinite plane.

We thus see that the structure of the EMI on the torus is richer than on the plane. In order to obtain a viable EMI ansatz, we shall construct a C -function that extends Eq. (A2) to the torus in a simple way. In Section A 5, we construct a second EMI ansatz using a different $C(\mathbf{r})$, which has very similar properties to the first

one. This fact, together with the excellent agreement with the numerical data for the boson and Dirac fermion on the lattice, show the robustness and utility of the EMI construction.

1. Infinite cylinder

Let us begin with the simpler case where the entire space takes the topology of an infinite cylinder with circumference L_y , Fig. 5a.

a. Semi-infinite region A

We first take the region A to be a semi-infinite cylinder which ends at $x = 0$. The entangling surface is a circle, and constitutes the domain of integration in the EMI calculation. The expression for the EE entropy reads

$$S = \int_0^{L_y} dy_1 \int_0^{L_y} dy_2 \hat{n}_1 \cdot \hat{n}_2 C(\mathbf{r}_1 - \mathbf{r}_2) \quad (\text{A5})$$

$$= \int_0^{L_y} dy_1 \int_0^{L_y} dy_2 s_1 \frac{\hat{x} \cdot \hat{x}}{\tilde{y}_{12}^2}, \quad (\text{A6})$$

where we have defined $y_{12} = y_1 - y_2$, and

$$|\tilde{y}| = \begin{cases} |y|, & \text{if } |y| \leq L_y/2 \\ L_y - |y|, & \text{if } L_y/2 < |y| \leq L_y, \end{cases} \quad (\text{A7})$$

Eq. (A7) defines a rather simple distance function on a line segment with periodic boundary conditions, *i.e.* a (“flat”) circle. This constitutes our minimal prescription in modifying Eq. (A2) to account for the periodicity in the y -direction. We shall see that this ansatz yields sensible and transparent answers for the EE. In fact, our results for the EE on the cylinder and torus topologies will be shown to satisfy all the known requirements (see main text). Further, they will provide very accurate candidate functions to compare with numerical data for non-interacting bosons and fermions.

In obtaining Eq. (A6), we have used the fact that both normal vectors are $\hat{\mathbf{n}}_{1,2} = \hat{x}$, and $x_{1,2} = 0$ on the entangling surface. We change variables to $Y = (y_1 + y_2)/2$ and y_{12} , and perform the integral over Y :

$$S = s_1 L_y \int_{-L_y}^{L_y} \frac{dy_{12}}{\tilde{y}_{12}^2} = s_1 L_y 4 \int_{\delta}^{L_y/2} \frac{dy_{12}}{y_{12}^2}, \quad (\text{A8})$$

where in the last equality we have used the definition of \tilde{y}_{12} , Eq. (A7). We also introduced a UV cutoff δ to make the integral finite. The final result for the EE in the limit $L_y \gg \delta$ reads

$$S = \mathcal{B} \frac{L_y}{\delta} - \gamma + \dots, \quad (\text{A9})$$

where $\mathcal{B} = 4s_1$, and $\gamma = 8s_1$. Both constants are positive since $s_1 > 0$. We have thus recovered the boundary law term, and a universal (negative) contribution $-\gamma$.

b. Finite region A

Let us now consider the more interesting case where the subregion A is a cylinder of finite length L_A , as shown in Fig. 5b. The boundary of region A is now composed of 2 disjoint circles (left and right): $\partial A = L \cup R$. The EE computed within the EMI will thus be composed of 4 contributions, depending on whether \mathbf{r}_i lies on the left or right circle:

$$\begin{aligned} S &= S^{LL} + S^{RR} + S^{LR} + S^{RL} \\ &= 2S^{RR} + 2S^{RL}. \end{aligned} \quad (\text{A10})$$

In the last equality we have used the translation symmetry along the x -direction. Now, S^{RR} is exactly given by the semi-infinite cylinder answer, Eq. (A9). It remains to compute S^{RL} :

$$S^{RL} = \int_0^{L_y} dy_1 \int_0^{L_y} dy_2 \frac{-s_1}{L_A^2 + \tilde{y}_{12}^2}, \quad (\text{A11})$$

where we have used $\hat{\mathbf{n}}_1 = -\hat{\mathbf{n}}_2$ when $\mathbf{r}_{1,2}$ do not lie on the same circle (disconnected component of ∂A). By again changing variables to Y and y_{12} , and performing the integrals we obtain

$$S^{RL} = -s_1 \frac{4L_y}{L_A} \cot^{-1} \left(\frac{2L_A}{L_y} \right). \quad (\text{A12})$$

Note that this result is entirely independent of the cutoff δ . The final answer for the EE of A thus reads:

$$S = \mathcal{B} \frac{2L_y}{\delta} - \chi^{\text{cyl}} + \dots, \quad (\text{A13})$$

where we have defined the cylinder function $\chi^{\text{cyl}}(L_A/L_y)$,

$$\chi^{\text{cyl}} = 2\gamma + \frac{2\kappa}{\pi} \frac{L_y}{L_A} \cot^{-1} \left(\frac{2L_A}{L_y} \right), \quad (\text{A14})$$

which depends on the single dimensionless ratio, L_A/L_y . Here $\kappa = 4\pi s_1$ is the “thin strip” constant: It determines the subleading term in the EE of a thin strip of width L_A in the infinite plane,³⁰

$$S_{\text{strip}} = \mathcal{B} \frac{2L}{\delta} - \kappa \frac{L}{L_A} + \dots, \quad (\text{A15})$$

where L is a long-distance regulator for region A . \mathcal{B} and γ are as above, in particular $\gamma = 8s_1$.

2. Torus in 2d

We can now tackle the torus topology in 2d, Fig. 5c. The extra complication compared with the infinite cylinder is that the space is now periodic in the x -direction. As a result the final answer must be the same under the exchange $L_A \leftrightarrow L_x - L_A$ (by purity). The structure of the EE within in the EMI will still decompose into 2 terms, as

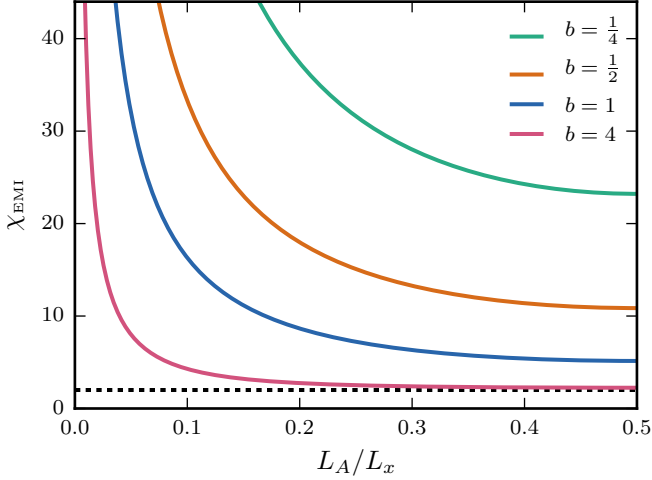


FIG. 6. Full χ_{EMI} (no vertical offset) for different aspect ratios (using $s_1 = 1/8$). From bottom to top: $L_x/L_y = 4, 1, 1/2, 1/4$. The horizontal dashed line corresponds to $L_x/L_y = \infty$, in which case $\chi_{\text{EMI}} = 2\gamma = 2$.

in Eq. (A10). S_{RR} will be the same as in the cylinder calculation above because it is not sensitive to the x -cycle. In contrast, S_{RL} does know about the x -cycle. The simplest way to accommodate for this is to add a “mirror” contribution to Eq. (A2), $C^{\text{mirror}} = s_1/[(L_x - L_A)^2 + \tilde{y}_{12}^2]$, in the calculation of $S^{RL} = S^{LR}$. Performing the calculation with the additional mirror term, we finally obtain

$$S = \mathcal{B} \frac{L_y}{\delta} - \chi_{\text{EMI}} + \dots, \quad (\text{A16})$$

where the torus EE function is

$$\chi_{\text{EMI}} = 2\gamma + \frac{2\kappa L_y}{\pi} \left[\frac{\cot^{-1}\left(\frac{2L_A}{L_y}\right)}{L_A} + \frac{\cot^{-1}\left(\frac{2(L_x - L_A)}{L_y}\right)}{L_x - L_A} \right] \quad (\text{A17})$$

and $\mathcal{B} = 4s_1$, $\gamma = 8s_1$ and $\kappa = 4\pi s_1$ are the same constants as in the infinite cylinder calculations above. \mathcal{B} is independent of the aspect ratio of the torus. Further, χ_{EMI} is non-negative. Fig. 6 shows the b, θ -dependence of χ_{EMI} .

3. Torus in 3d

We now turn to the torus topology in 3d, see Fig. 4. We compactify the spatial dimensions such that the i th coordinate r_i is identified with $r_i + L_i$, $i = x, y, z$. The entangling surface consists of 2 disconnected parts, each

of which is a 2-torus. As a result, the EE within the EMI again decomposes into 2 terms as in Eq. (A10). The first term, S^{RR} , comes from having \mathbf{r}_1 and \mathbf{r}_2 both on the right 2-torus R :

$$S^{RR} = \int dy_1 dz_1 \int dy_2 dz_2 \frac{s_1}{(\tilde{y}_{12}^2 + \tilde{z}_{12}^2)^2}, \quad (\text{A18})$$

where \tilde{y}_{12} is as defined in Eq. (A7), \tilde{z}_{12} is analogously defined but with L_z instead of L_y . We change integration variables to $Y = (y_1 + y_2)/2$, y_{12} , and $Z = (z_1 + z_2)/2$, z_{12} , and perform the integrals over Y, Z :

$$S^{RR} = 16L_y L_z \int_0^{L_y/2} dy_{12} \int_0^{L_z/2} dz_{12} \frac{s_1}{(y_{12}^2 + z_{12}^2)^2}, \quad (\text{A19})$$

where we were able to remove the tildes by restricting the domain of integration. Performing both integrals we get

$$S^{RR} = 2\pi s_1 \frac{L_y L_z}{\delta^2} - 16s_1 \left[1 + \frac{L_y}{L_z} \tan^{-1}\left(\frac{L_y}{L_z}\right) + \frac{L_z}{L_y} \tan^{-1}\left(\frac{L_z}{L_y}\right) \right] + O(\delta/L_{y,z}), \quad (\text{A20})$$

which is symmetric under $L_y \leftrightarrow L_z$, as expected. The term in brackets is independent of the UV cutoff δ , and will contribute to the torus function χ_{EMI}^{3d} .

Next, we turn to the S^{RL} term in Eq. (A10). As in the 2d torus calculation, S^{RL} will receive a contribution from a term with $|x_{12}| = L_A$, and from a “mirror” term with $|x_{12}| = L_x - L_A$, in order to account for the periodicity along x . The first contribution reads

$$S_{(1)}^{RL} = \int dy_1 dz_1 \int dy_2 dz_2 \frac{-s_1}{(L_A^2 + \tilde{y}_{12}^2 + \tilde{z}_{12}^2)^2}, \quad (\text{A21})$$

where we have used $\hat{\mathbf{n}}_1 = -\hat{\mathbf{n}}_2$. Again changing variables to center-of-mass and relative coordinates, and performing the integration over the former we get

$$S_{(1)}^{RL} = \int_0^{L_y/2} dy_{12} \int_0^{L_z/2} dz_{12} \frac{-16L_y L_z s_1}{(L_A^2 + y_{12}^2 + z_{12}^2)^2} \quad (\text{A22})$$

$$= -\frac{16L_y L_z s_1}{2L_A^2} \left[\frac{L_y \tan^{-1}\left(\frac{L_z}{\sqrt{4L_A^2 + L_y^2}}\right)}{\sqrt{4L_A^2 + L_y^2}} + y \leftrightarrow z \right].$$

Thus the final answer for the EE is

$$S = \mathcal{B} \frac{2L_y L_z}{\delta^2} - \chi_{\text{EMI}}^{3d} + \dots, \quad (\text{A23})$$

where

$$\chi_{\text{EMI}}^{3d} = 2\gamma^{3d} + \frac{4\kappa^{3d}}{\pi} \left[\frac{L_y}{L_z} \tan^{-1} \left(\frac{L_y}{L_z} \right) + \frac{L_y L_z}{2L_A^2} \frac{L_y \tan^{-1} \left(\frac{L_z}{\sqrt{4L_A^2 + L_y^2}} \right)}{\sqrt{4L_A^2 + L_y^2}} \right. \\ \left. + \frac{L_y L_z}{2(L_x - L_A)^2} \frac{L_y \tan^{-1} \left(\frac{L_z}{\sqrt{4(L_x - L_A)^2 + L_y^2}} \right)}{\sqrt{4(L_x - L_A)^2 + L_y^2}} + y \leftrightarrow z \right] \quad (\text{A24})$$

with $\gamma^{3d} = 16s_1$ and $\kappa^{3d} = 8\pi s_1$. We note that the square brackets contain 6 terms due to the contributions with y and z interchanged. Thus, χ_{EMI}^{3d} is fully symmetric under the exchange $L_y \leftrightarrow L_z$, as it should be. We have defined κ^{3d} as the thin slab coefficient:

$$\lim_{L_A \rightarrow 0} \chi_{\text{EMI}} = \kappa^{3d} \frac{L_y L_z}{L_A^2}, \quad (\text{A25})$$

which is readily obtained from Eq. (A24) by using the identity $\tan^{-1} z + \tan^{-1}(1/z) = \pi/2$, with $z > 0$. The result simplifies for $b_y = b_z = b$ to give

$$\chi_{\text{EMI}}^{3d}(\theta) = 16\pi\kappa^{3d} \left[\frac{1}{8\pi} + \frac{\cot^{-1} \sqrt{1 + (b\theta/\pi)^2}}{b^2 \theta^2 \sqrt{1 + (b\theta/\pi)^2}} \right. \\ \left. + \frac{\cot^{-1} \sqrt{1 + b^2(2\pi - \theta)^2/\pi^2}}{b^2(2\pi - \theta)^2 \sqrt{1 + b^2(2\pi - \theta)^2/\pi^2}} \right] + 2\gamma^{3d}. \quad (\text{A26})$$

This is the case we study numerically in Fig. 4 of the main text for the non-interacting gapless boson. We note that χ_{EMI}^{3d} has a similar structure to the 2d result, *e.g.* the appearance of \cot^{-1} .

4. Properties in 2d

a. Special scaling for $b \leq 1$

We discuss the special scaling encountered for $b \cdot \chi_{\text{EMI}}(\theta)$, relative to its value at $\theta = \pi$:

$$\tilde{\chi}_{\text{EMI}}(\theta) = \frac{b}{2\pi} [\chi_{\text{EMI}}(\theta; b) - \chi_{\text{EMI}}(\pi; b)] \quad (\text{A27}) \\ = \frac{4\kappa}{\pi} \left(\frac{\cot^{-1}(b\theta/\pi)}{\theta} + \frac{\cot^{-1}(b(2\pi - \theta)/\pi)}{2\pi - \theta} \right. \\ \left. - \frac{2}{\pi} \cot^{-1} b \right). \quad (\text{A28})$$

As was mentioned in the main text, $\tilde{\chi}_{\text{EMI}}$ is approximately independent of the aspect ratio b in the range $b \leq 1$. Fig. 7 demonstrates that this statement holds very accurately.

We note that in the $b \rightarrow 0$ limit

$$\tilde{\chi}_{\text{EMI}}(\theta; 0) = \frac{2\kappa}{\pi} \frac{(\pi - \theta)^2}{\theta(2\pi - \theta)}. \quad (\text{A29})$$

We recognize this as precisely the corner EE function $a(\theta)$ of the family of Lifshitz quantum critical points with conformal wavefunctions^{13!} For that family of $z = 2$ theories,⁴⁷ $\kappa = \pi c/24$,^{13,53} where c is the Virasoro central charge of the parent 1d CFT that describes the equal-time correlations of the theory. At present, we do not have an explanation for the appearance of this corner function in the torus EE of the EMI. We note that the latter has a different corner function $a_{\text{EMI}}(\theta)$.^{43,44}

b. Smooth and thin-torus limit expansions

We here give the leading terms in the smooth $\theta \approx \pi$ and thin slice $\theta \approx 0$ expansions for χ_{EMI} in 2d. In the smooth limit we get

$$\chi_{\text{EMI}}(\theta \approx \pi) = \left(2\gamma + \frac{8\kappa \cot^{-1} b}{\pi b} \right) \\ + \frac{8\kappa \left(b + 2b^3 + (b^2 + 1)^2 \cot^{-1} b \right)}{\pi^3 b (b^2 + 1)^2} (\theta - \pi)^2 + O(\theta - \pi)^4 \quad (\text{A30})$$

while in the thin slice limit we get

$$\chi_{\text{EMI}}(\theta \approx 0) = \frac{2\pi\kappa}{b\theta} + \left(2\gamma + \frac{2\kappa \cot^{-1}(2b)}{\pi b} - \frac{4\kappa}{\pi} \right) + O(\theta). \quad (\text{A31})$$

We see that the first term matches the thin strip contribution, as described above and in the main text.

5. Another ansatz

The reader might wonder how generic is the ansatz described in the above sections? Indeed, one could have chosen another ansatz for the $C(\mathbf{r})$ function in Eq. (A1). Here, we introduce another ansatz, and show that it has

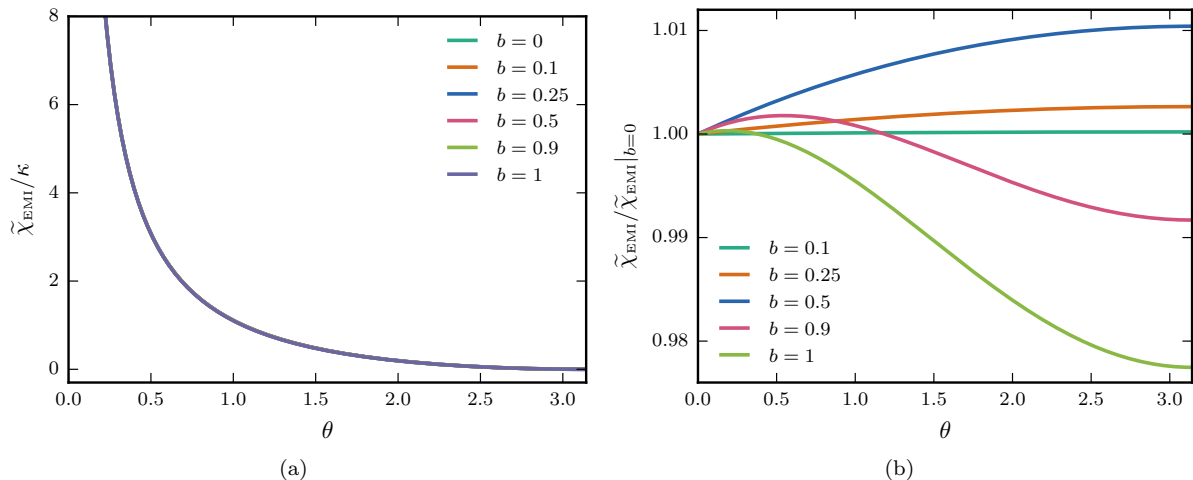


FIG. 7. **a)** $\tilde{\chi}_{\text{EMI}}(\theta)/\kappa$ for different aspect ratios b . The curves are plotted in different colors but cannot be distinguished in this plot. **b)** For the same values of b as in a), we plot $\tilde{\chi}_{\text{EMI}}$ divided by its value at $b=0$, $\tilde{\chi}_{\text{EMI}}(\theta; b)/\tilde{\chi}_{\text{EMI}}(\theta; 0)$. Note the very narrow ordinate range!

very similar properties to the first one. We focus on $d = 2$, where the new ansatz for the C -function reads:

$$C(\mathbf{r}) = \frac{s_1}{\text{ch}(x)^2 + \text{ch}(y)^2} \quad (\text{A32})$$

where

$$\text{ch}(r_i) = \frac{L_i}{\pi} \sin\left(\frac{\pi r_i}{L_i}\right) \quad (\text{A33})$$

is the chord length on a circle of circumference L_i . Eq. (A32) is manifestly periodic under $r_i \rightarrow r_i + L_i$, and reduces to Eq. (A2) at short distances. The resulting torus function χ can be easily obtained using Eq. (A1):

$$\chi(\theta; b) = \frac{\pi\kappa}{b \sin(\theta/2) \sqrt{1 + b^2 \sin^2(\theta/2)}}. \quad (\text{A34})$$

This new ansatz, just like the original one, obeys all the known physical constraints required for χ , such as being convex decreasing on $[0, \pi)$, and the reflection property $\chi(2\pi - \theta) = \chi(\theta)$. Further, in Fig. 8 we quantitatively compare the new ansatz with the old one, using $\chi(\theta) - \chi(\pi)$ normalized by κ . This is the same quantity that is compared with the boson and fermion numerical data in the main text. We see that the deviations are very small.

Appendix B: Numerical calculations

We calculate the EE for the lattice Hamiltonian of a free relativistic boson in the massless limit, which is given

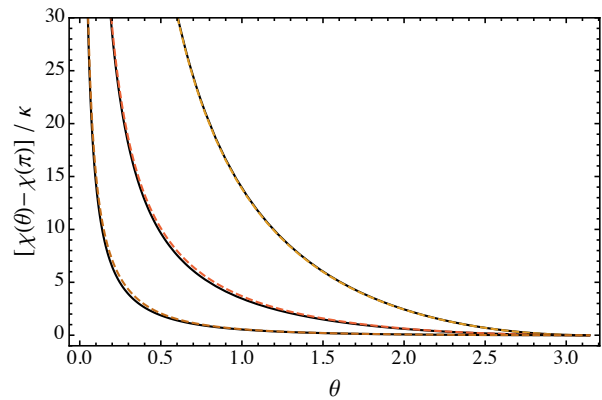


FIG. 8. We compare the new EMI ansatz (dashed) with the old one (black and solid) for 3 different aspect ratios. Top to bottom: $b = 1/4, 1, 4$.

by

$$H = \frac{1}{2} \sum_{\mathbf{x}} \left[\pi_{\mathbf{x}}^2 + (\phi_{x_1+1, x_2, \dots, x_d} - \phi_{\mathbf{x}})^2 + \dots + (\phi_{x_1, x_2, \dots, x_d+1} - \phi_{\mathbf{x}})^2 \right], \quad (\text{B1})$$

where d is the spatial dimension of the lattice, $\mathbf{x} = (x_1, x_2, \dots, x_d)$ represents the spatial lattice coordinates, each x_i is summed from 1 to L_i , and L_i is the lattice length along the i^{th} dimension.

For translationally invariant boundary conditions, the two-point vacuum correlation functions corresponding to

this Hamiltonian are given by

$$\begin{aligned}\langle\phi_0\phi_{\mathbf{x}}\rangle &= \frac{1}{2N} \sum_{\mathbf{k}} \frac{1}{\omega_{\mathbf{k}}} \cos(k_1x_1) \cos(k_2x_2) \cdots \cos(k_dx_d), \\ \langle\pi_0\pi_{\mathbf{x}}\rangle &= \frac{1}{2N} \sum_{\mathbf{k}} \omega_{\mathbf{k}} \cos(k_1x_1) \cos(k_2x_2) \cdots \cos(k_dx_d),\end{aligned}\tag{B2}$$

where $N = L_1L_2 \cdots L_d$ is the total number of lattice sites and

$$\omega_{\mathbf{k}} = 2\sqrt{\sin^2(k_1/2) + \sin^2(k_2/2) + \dots + \sin^2(k_d/2)}.\tag{B3}$$

The values of the momenta \mathbf{k} are quantized such that $k_i = 2n_i\pi/L_i$ when the lattice has PBC along the i^{th} lattice direction and similarly $k_i = (2n_i + 1)\pi/L_i$ for APBC (where $n_i = 0, 1, \dots, L_i - 1$).

Note that, for a fully periodic lattice, the correlator $\langle\phi_0\phi_{\mathbf{x}}\rangle$ (and, as we will see, the EE) diverges since $\omega_{\mathbf{k}} = 0$ for the zero mode $\mathbf{k} = 0$. In order to avoid this divergence, our calculations impose APBC along the y -

direction (*i.e.* the x_2 -direction) and PBC along the remaining lattice directions. In doing so, we have $\omega_{\mathbf{k}} \neq 0$ for all allowed values of \mathbf{k} .

These two-point correlators define the $N \times N$ matrices $X_{ab} = \langle\phi_{\mathbf{x}_a}\phi_{\mathbf{x}_b}\rangle = \langle\phi_0\phi_{\mathbf{x}_b - \mathbf{x}_a}\rangle$ and $P_{ab} = \langle\pi_0\pi_{\mathbf{x}_b - \mathbf{x}_a}\rangle$, where a, b label lattice sites. To get $S(A)$ we only need to know the smaller $N_A \times N_A$ matrices X_A and P_A , which are the sections of X and P (respectively) with indices i, j restricted to the N_A sites of region A .⁴⁵ The EE is given in terms of the eigenvalues ν_ℓ of $\sqrt{X_A P_A}$ as⁵⁴

$$S(A) = \sum_{\ell=1}^{N_A} \left[\left(\nu_\ell + \frac{1}{2} \right) \log \left(\nu_\ell + \frac{1}{2} \right) - \left(\nu_\ell - \frac{1}{2} \right) \log \left(\nu_\ell - \frac{1}{2} \right) \right].\tag{B4}$$

In order to access the EE on larger lattices, for the case of the torus geometry we employ an extension of the above methods as given in Ref. 21 that takes advantage of the translational symmetry along $(d - 1)$ spatial lattice directions. In this modified method, we map the $(d + 1)$ -dimensional model to an effective model consisting of $L_2 \times L_3 \times \dots \times L_d$ separate $(1 + 1)$ -dimensional chains.

-
- ¹ P. Calabrese and J. L. Cardy, *J. Stat. Mech.* **0406**, P06002 (2004), hep-th/0405152.
- ² H. Casini and M. Huerta, *J. Phys.* **A42**, 504007 (2009), 0905.2562.
- ³ E. Fradkin, *Field Theories of Condensed Matter Physics*, *Field Theories of Condensed Matter Physics* (Cambridge University Press, 2013), ISBN 9780521764445.
- ⁴ B. Zeng, X. Chen, D.-L. Zhou, and X.-G. Wen, *ArXiv e-prints* (2015), 1508.02595.
- ⁵ N. Laflorencie, *ArXiv e-prints* (2015), 1512.03388.
- ⁶ S. Dong, E. Fradkin, R. G. Leigh, and S. Nowling, *Journal of High Energy Physics* **5**, 016 (2008), 0802.3231.
- ⁷ Y. Zhang, T. Grover, A. Turner, M. Oshikawa, and A. Vishwanath, *Phys. Rev. B* **85**, 235151 (2012), 1111.2342.
- ⁸ L. Cincio and G. Vidal, *Phys. Rev. Lett.* **110**, 067208 (2013).
- ⁹ S. V. Isakov, M. B. Hastings, and R. G. Melko, *Nature Physics* **7**, 772 (2011), 1102.1721.
- ¹⁰ Y.-F. Wang, Z.-C. Gu, C.-D. Gong, and D. N. Sheng, *Physical Review Letters* **107**, 146803 (2011), 1103.1686.
- ¹¹ H.-C. Jiang, Z. Wang, and L. Balents, *Nature Physics* **8**, 902 (2012), 1205.4289.
- ¹² S. Depenbrock, I. P. McCulloch, and U. Schollwöck, *Phys. Rev. Lett.* **109**, 067201 (2012).
- ¹³ E. Fradkin and J. E. Moore, *Physical Review Letters* **97**, 050404 (2006), cond-mat/0605683.
- ¹⁴ J.-M. Stéphan, S. Furukawa, G. Misguich, and V. Pasquier, *Phys. Rev. B* **80**, 184421 (2009), 0906.1153.
- ¹⁵ B. Hsu, M. Mulligan, E. Fradkin, and E.-A. Kim, *Phys. Rev. B* **79**, 115421 (2009), 0812.0203.
- ¹⁶ M. A. Metlitski, C. A. Fuertes, and S. Sachdev, *Phys. Rev. B* **80**, 115122 (2009), 0904.4477.
- ¹⁷ B. Hsu and E. Fradkin, *Journal of Statistical Mechanics: Theory and Experiment* **9**, 09004 (2010), 1006.1361.
- ¹⁸ M. Oshikawa, *ArXiv e-prints* (2010), 1007.3739.
- ¹⁹ M. A. Metlitski and T. Grover, *ArXiv e-prints* (2011), 1112.5166.
- ²⁰ B. Swingle and T. Senthil, *Phys. Rev. B* **86**, 155131 (2012), 1109.3185.
- ²¹ X. Chen, G. Y. Cho, T. Faulkner, and E. Fradkin, *Journal of Statistical Mechanics: Theory and Experiment* **2**, 02010 (2015), 1412.3546.
- ²² M. Pretko and T. Senthil, *ArXiv e-prints* (2015), 1510.03863.
- ²³ H. Ju, A. B. Kallin, P. Fendley, M. B. Hastings, and R. G. Melko, *Phys. Rev. B* **85**, 165121 (2012).
- ²⁴ S. Inglis and R. G. Melko, *New Journal of Physics* **15**, 073048 (2013).
- ²⁵ B. Kulchytsky, C. M. Herdman, S. Inglis, and R. G. Melko, *Phys. Rev. B* **92**, 115146 (2015).
- ²⁶ J. Helmes and S. Wessel, *Phys. Rev. B* **89**, 245120 (2014).
- ²⁷ D. J. Luitz, X. Plat, F. Alet, and N. Laflorencie, *Phys. Rev. B* **91**, 155145 (2015).
- ²⁸ N. Laflorencie, D. J. Luitz, and F. Alet, *Phys. Rev. B* **92**, 115126 (2015).
- ²⁹ E. H. Lieb and M. B. Ruskai, *Journal of Mathematical Physics* **14** (1973).
- ³⁰ H. Casini and M. Huerta, *J. Phys.* **A42**, 504007 (2009), 0905.2562.
- ³¹ H. Casini and M. Huerta, *Nucl. Phys.* **B764**, 183 (2007), hep-th/0606256.
- ³² T. Hirata and T. Takayanagi, *JHEP* **02**, 042 (2007), hep-th/0608213.
- ³³ A. B. Kallin, K. Hyatt, R. R. P. Singh, and R. G. Melko, *Physical Review Letters* **110**, 135702 (2013), 1212.5269.

- ³⁴ A. B. Kallin, E. M. Stoudenmire, P. Fendley, R. R. P. Singh, and R. G. Melko, *Journal of Statistical Mechanics: Theory and Experiment* **2014**, P06009 (2014).
- ³⁵ P. Bueno, R. C. Myers, and W. Witczak-Krempa, *Physical Review Letters* **115**, 021602 (2015), 1505.04804.
- ³⁶ P. Bueno, R. C. Myers, and W. Witczak-Krempa, *Journal of High Energy Physics* **9**, 91 (2015), 1507.06997.
- ³⁷ E. M. Stoudenmire, P. Gustainis, R. Johal, S. Wessel, and R. G. Melko, *Phys. Rev.* **B90**, 235106 (2014).
- ³⁸ J. Helmes and S. Wessel, *Phys. Rev. B* **92**, 125120 (2015), 1411.7773.
- ³⁹ J. Helmes, L. E. Hayward Sierens, A. Chandran, W. Witczak-Krempa, and R. G. Melko, *Phys. Rev. B* **94**, 125142 (2016).
- ⁴⁰ P. Bueno and R. C. Myers, *JHEP* **08**, 068 (2015), 1505.07842.
- ⁴¹ T. Faulkner, R. G. Leigh, and O. Parrikar, *Journal of High Energy Physics* **4**, 88 (2016), 1511.05179.
- ⁴² H. Casini, C. D. Fosco, and M. Huerta, *J. Stat. Mech.* **0507**, P07007 (2005), cond-mat/0505563.
- ⁴³ H. Casini and M. Huerta, *JHEP* **03**, 048 (2009), 0812.1773.
- ⁴⁴ B. Swingle (2010), 1010.4038.
- ⁴⁵ I. Peschel, *J. Phys. A: Math. Gen.* **36**, L205 (2003).
- ⁴⁶ J.-M. Stéphan, H. Ju, P. Fendley, and R. G. Melko, *New Journal of Physics* **15**, 015004 (2013), 1207.3820.
- ⁴⁷ E. Ardonne, P. Fendley, and E. Fradkin, *Annals of Physics* **310**, 493 (2004), cond-mat/0311466.
- ⁴⁸ W. Witczak-Krempa *et. al.* (in preparation).
- ⁴⁹ A. Kitaev, *Annals of Physics* **321**, 2 (2006), cond-mat/0506438.
- ⁵⁰ H. Yao and X.-L. Qi, *Physical Review Letters* **105**, 080501 (2010), 1001.1165.
- ⁵¹ R. C. Myers and A. Sinha, *Phys. Rev. D* **82**, 046006 (2010), 1006.1263.
- ⁵² H. Casini and M. Huerta, *Phys. Rev. D* **85**, 125016 (2012), 1202.5650.
- ⁵³ P. Bueno and W. Witczak-Krempa, *Phys. Rev. B* **93**, 045131 (2016), 1511.04077.
- ⁵⁴ H. Casini and M. Huerta, *Journal of Physics A: Mathematical and Theoretical* **42**, 504007 (2009).